ACS APPLIED MATERIALS & INTERFACES

Research Article

www.acsami.org

Purine-Stabilized Green Fluorescent Gold Nanoclusters for Cell Nuclei Imaging Applications

V. Venkatesh,[†] Akansha Shukla,[‡] Sri Sivakumar,*[,‡,§] and Sandeep Verma*[,†,§]

[†]Department of Chemistry, [‡]Department of Chemical Engineering, Material Science Programme, and [§]DST Thematic Unit of Excellence on Soft Nanofabrication, Indian Institute of Technology Kanpur, Kanpur, Uttar Pradesh 208016, India

Supporting Information

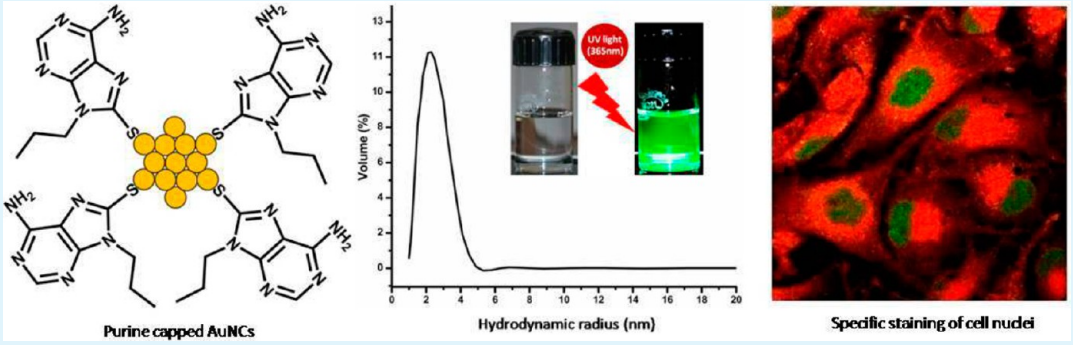

ABSTRACT: We report facile one-pot synthesis of water-soluble green fluorescent gold nanoclusters (AuNCs), capped with 8-mercapto-9-propyladenine. The synthesized AuNCs were characterized by Fourier transform infrared (FTIR), powder X-ray diffraction (PXRD), transmission electron microscopy (TEM), ^{1}H NMR, and matrix-assisted laser desorption/ionization time-of-flight (MALDI-TOF) mass spectrometry. These nanoclusters show high photostability and biocompatibility. We observed that AuNCs stain cell nuclei with high specificity, where the mechanism of AuNC uptake was established through pathway-specific uptake inhibitors. These studies revealed that cell internalization of AuNCs occurs via a macropinocytosis pathway.

KEYWORDS: *gold nanoclusters, nuclei imaging, green fluorescence, HeLa cells, macropinocytosis*

1. INTRODUCTION

It is important to visualize various cellular compartments or to study cellular processes for a number of biological studies. It is often very difficult to distinguish different cellular compartments by simple optical microscopy, thus specific staining of cellular compartments is highly desirable for imaging subcellular structures. In particular, imaging of the nucleus is highly important as it contains the genetic material of the cell and is the location for DNA replication and drug−DNA interactions, to name a few.[1]

Silver nanoclusters (AgNCs), gold nanoclusters (AuNCs), quantum dots (QDs), lanthanide-doped nanomaterials, and organic dyes have emerged as important classes of luminescent materials available for biolabeling and imaging applications.[2−7] QDs have attracted much attention because of their unique optical properties (high extinction coefficient) and stable emission signals. Unfortunately, they are prepared from highly toxic inorganic substances such as cadmium, lead, selenium, and tellurium, and their use may be undesirable in certain in vivo systems due to issues of biocompatibility.[8,9] On the other hand, photobleaching of organic dyes hampers their utility for imaging applications.[10] Further, lanthanide ions also suffer from lesser absorption coefficients, which reduces their luminescence efficiency.

Among noble metal nanoclusters, AuNCs are more stable to oxidation and provide stable fluorescence as compared to AgNCs.[11] In addition, they can also be prepared in ultrafine size with superior biocompatibility.[12] Various thiol-capped AuNCs have been synthesized, and their applications in catalysis, luminescence, and chemical sensing were extensively studied.[13−18] Crystal structures of Au_{13}, Au_{20}, Au_{25}, Au_{38}, and Au_{102} are reported, and their luminescence properties have revealed that cluster size and nature of capping agents influence emission properties.[19−23]

Biomolecules such as protein, oligonucleotide, enzyme, and peptide capped AuNCs are increasingly used because of their nontoxic and biocompatible nature.[24−29] For example, glutathione-stabilized gold nanoclusters were synthesized, and their luminescent property in the visible region was utilized for biosensing applications.[30,31] Polycytosine and polyadenine DNA as templates for gold nanocluster preparation were recently reported.[32] Our group has also recently described thiolated tryptophan-based gold nanoclusters for imaging *Caenorhabditis elegans*.[33]

Received: November 25, 2013
Accepted: January 20, 2014
Published: January 20, 2014

Scheme 1. Synthesis of 8-Mercapto-9-propyladenine (1) Capped Fluorescent Gold Nanoclusters[a]

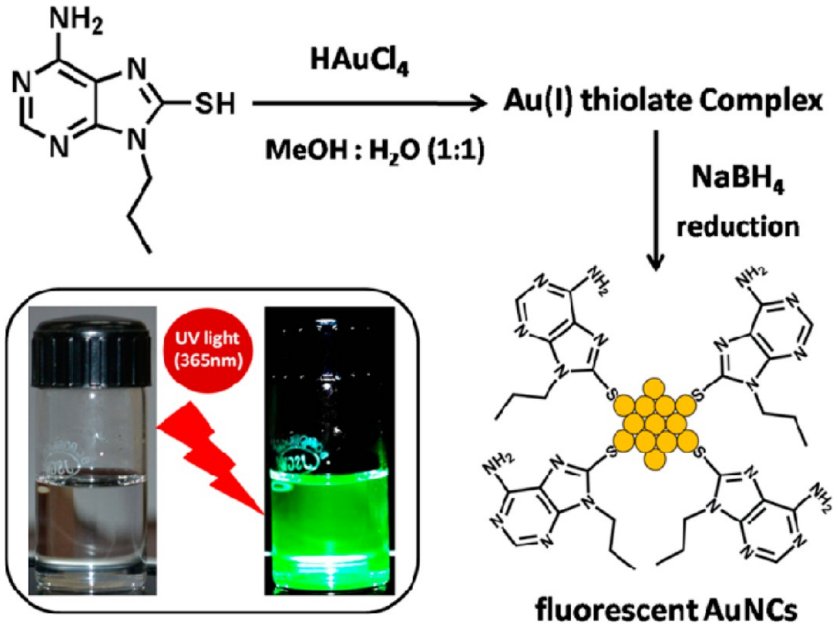

[a]Inset: capped AuNCs emit bright green fluorescence when excited with an UV hand light (365 nm).

Herein, we report the synthesis of biocompatible, ultrafine AuNCs stabilized with modified purine base, 8-mercapto-9-propyladenine. As an application, we show that these AuNCs could stain nuclei in four different cell lines. The synthetic procedure for the preparation of stabilized AuNCs is given in Scheme 1. 8-Mercapto-9-propyladenine was treated with chloroauric acid to afford a yellow colored solution, which eventually resulted in the formation of a white precipitate after 2 h. This transformation is suggestive of Au(III) to Au(I) reduction, followed by Au(I)−thiolate complex formation. The intermediate Au(I)−thiolate complex was reduced with sodium borohydride to form AuNCs, which were separated by centrifugation. We noted that capped AuNCs are stable for several months, without losing their fluorescence property (Supporting Information).

2. EXPERIMENTAL SECTION

2.1. Synthesis of 8-Bromo-9-propyladenine. Synthesis of 8-bromo-9-propyladenine has been reported.[34] A similar protocol was followed, and product purity was confirmed using standard spectroscopic techniques.

2.2. Synthesis of 8-Mercapto-9-propyladenine (1). The titled compound was prepared by following a modified literature procedure.[35] 8-Bromo-9-propyladenine (800 mg, 3.12 mmol) was refluxed with thiourea (472 mg, 6.20 mmol) in 25 mL of ethanol, under a nitrogen atmosphere for 24 h. The reaction mixture was evaporated and dried under high vacuum. The residue was partitioned between ethyl acetate and H_2O. The extracted organic layer was dried and subjected to silica gel column chromatography eluting with MeOH/$CHCl_3$ (2:98) to afford the desired compound as a white powder (463 mg, 71% yield). HRMS: $[M + H]^+$ calculated, 210.0813; found, 210.0818. ^{1}H NMR (500 MHz, DMSO-d_6, 25 °C, TMS): δ (ppm) 0.82 (t, 3H, CH_3), 1.71 (m, 2H, CH_2), 4.03 (t, 2H, CH_2), 6.81 (s, 2H, NH_2), 8.11 (s, 1H, C2−H), 12.27 (s, 1H, SH).

2.3. Synthesis of Fluorescent AuNCs. Synthesis of AuNCs was carried out by following a reported literature procedure with minor modifications.[36] 8-Mercapto-9-propyladenine-capped AuNCs were prepared by the reaction of **1** (50 mg, 0.23 mmol) with $HAuCl_4$ (20 mg, 0.059 mmol) in MeOH:H_2O (1:1) mixed solvent. A white colored precipitate appeared after addition of $HAuCl_4$, which was allowed to stir for 2 h at room temperature. This white-colored precipitate is formed due to the reduction of Au(III) into Au(I). Further reduction of the Au(I)−thiolate complex with $NaBH_4$ (51 mg, 1.35 mmol) resulted in the formation of AuNCs. The obtained solution was centrifuged to avoid bigger insoluble clusters. The clear solution so obtained was dried and washed with DMF to remove excess $NaBH_4$. AuNCs were dried under high vacuum and used for further experiments.

2.4. Characterizations. ^{1}H NMR spectra were obtained on a JEOL-DELTA2 500 model spectrometer operating at 500 MHz. The spectra were recorded in DMSO-d_6 solvent, and the chemical shifts were referenced with respect to tetramethylsilane. FTIR analyses were done for solid dry powder after making pellets with KBr on a Bruker Vector 22 FTIR spectrophotometer operating from 400 to 4000 cm^{-1}. High-resolution (ESI^+ mode) mass spectra were obtained from a WATERS HAB 213 machine. UV−vis absorption spectra were recorded on a Varian CARY 100 Bio UV−vis spectrophotometer (Varian Inc., USA), with 10 mm quartz cell at 25 ± 0.1 °C. Fluorescence emission spectra were recorded on a Varian CARY 100 Bio fluorescence spectrophotometer (Varian Inc., USA), with a 10 mm quartz cell at 25 ± 0.1 °C. Powder X-ray diffraction (PXRD) of AuNCs was performed with a PANalytical X'Pert PRO diffractometer with Cu Kα radiation (1.5405 Å), Netherlands. AuNCs were dissolved in methanol, and 5−10 μL of this sample was loaded over carbon-coated copper grids (Ted Pella, Inc., CA/US, 300 mesh). The sample was air-dried and subsequently examined under an FEI Technai 20 U Twin Transmission Electron Microscope. The microscope is a scanning transmission electron microscope (STEM), which is equipped with an EDS detector, HAADF detector, and Gatan digital imaging system. The MALDI spectrum for AuNCs was recorded after dissolving the cluster in methanol. Mass spectra were acquired on a time-of-flight mass spectrometer (MALDI-TOF-TOF Autoflex II TOF-TOF, Bruker Daltonics, Bremen, Germany) equipped with a nitrogen laser (λ = 337 nm). Scan accumulation and data processing were performed by using Flex Analysis 3.4 software. Sample preparation: Matrix solutions were freshly prepared: α-cyano-4-hydroxy-cinnamic acid (CHCA) was dissolved to saturation and sinapinic acid at 20 mg/mL in a H_2O/CH_3CN/HCOOH (50/50, 1%) solution. A 1:1 mixture of sample solution and matrix solution was mixed, and 0.5 μL of the resulting solution was used for analysis.

2.5. Cell Imaging with AuNCs. *Materials.* Dulbecco's modified eagle's medium (DMEM), trypsin-EDTA, penicillin-streptomycin

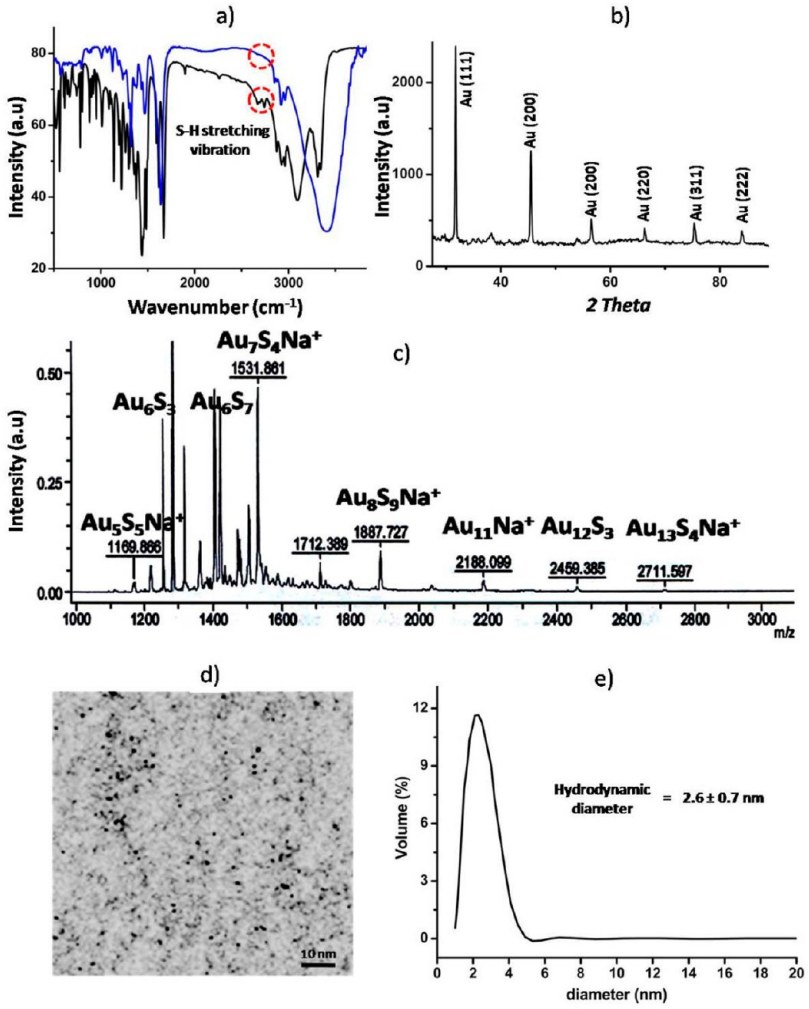

Figure 1. (a) FTIR spectrum of both 8-mercapto-9-propyladenine and the AuNC. The spectra clearly show the absence of S−H stretching at 2674 cm^{-1} after AuNC formation. (b) PXRD of as-synthesized AuNC shows the presence of fcc structure of metallic gold. (c) MALDI-TOF mass spectra of AuNCs show $[Au_{13}S_4Na]^+$ cluster formation along with fragmented peaks of $[Au_{12}S_3]$, $[Au_{11}Na]^+$, $[Au_8S_9Na]^+$, $[Au_7S_4Na]^+$ $[Au_6S_7]$, $[Au_6S_3]$, and $[Au_5S_5Na]^+$ clusters. (d) TEM images of AuNC. (e) Dynamic light-scattering measurement of AuNCs shows particles with hydrodynamic diameter of 2.6 ± 0.7 nm.

antibiotic, 3-(4,5-dimethylthiazol-2-yl)-2,5-diphenyltetrazolium bromide (MTT), bisbenzimide H 33258, and gelatin (from cold water fish skin) were purchased from Sigma Aldrich and used without further purification. Dimethyl sulfoxide (DMSO) was obtained from Merck Chemicals, India. Fetal bovine serum and CellMask Deep Red Plasma membrane stain were brought from Gibco Life technologies, India.

Cell Lines. In vitro studies were performed to characterize the biocompatibility of AuNCs, for this HeLa cell line (immortal cell line derived from cervical cancer) and A498 kidney cancer cell line were purchased from the National Center for Cell Sciences Pune, India. Schwann and L929 mouse fibroblast cell line were obtained from American Type Culture Collection (ATCC).

In Vitro Cell Viability/Cytotoxicity Studies. Cytotoxicity studies were done with sterilized AuNCs to determine if the nanoclusters can be used for biological applications. An MTT (3-(4,5-dimethylthiazol-2-yl)-2,5-diphenyltetrazolium bromide) assay was performed on four different cell lines (HeLa, A498, Schwann, and L929) to determine cell viability.

2.6. MTT Assay. To delineate biocompatibility of AuNCs, in vitro biocompatibility studies of AuNCs were carried out with HeLa, A498, Schwann, and L929 cells by MTT assay (Mosmann, 1983).[37] MTT assay is a quantitative colorimetric assay which assesses cell proliferation. Cells were maintained with Dulbecco's minimum essential medium supplemented with 10% fetal bovine serum in a humid incubator (37 °C and 5% CO_2). Cells (10^4 cells/well) were plated onto multiple glass-bottom tissue culture plates at an initial confluence of 70%. Cells were incubated with and without AuNCs for ∼24 h at 37 °C, in a 5% CO_2 humidified incubator followed by removal of media. An amount of 0.5 mg/mL of MTT in DMEM basal was prepared in a dark environment. After discarding the old media, 200 μL of the freshly prepared MTT solution was added to each of the cell-containing wells, followed by incubation for 4−5 h. After incubation, basal DMEM was removed, and DMSO (800 μL) was added. The viability of cells was determined by measuring their absorbance at 570 nm. All the in vitro cytotoxicity experiments were performed in quintuplicate, and out of it, the best three was taken to plot the MTT assay. The graph represents that AuNCs do not cause any acute cytotoxicity.

2.7. Cellular Uptake Studies. AuNCs were added to respective cell culture media at a concentration of 0.02 mg/mL. Treated cells (10^4 cells/well) were seeded on a sterilized glass coverslip (13 mm, 0.2% gelatin coated) for 15 h. AuNCs were added for an incubation time of ∼17 h, at 37 °C, with a 5% CO_2-humidified incubator. After this duration, incubated cells were washed thrice with PBS buffer and fixed with 4% formaldehyde solution for 20 min. After washing, cells were stained with deep red plasma membrane dye and washed with PBS buffer followed by nuclei staining with Hoechst 33258 for 20 min. The coverslips were then mounted on slides coated with buffered

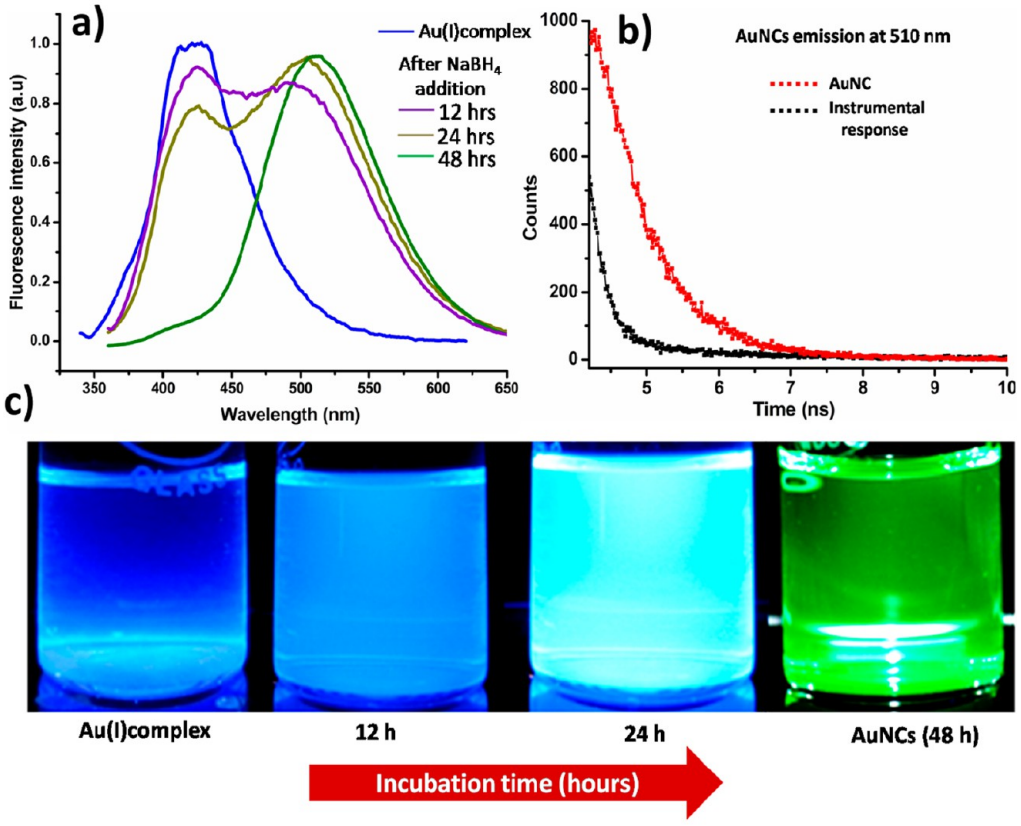

Figure 2. (a) Fluorescence emission spectra taken at different time intervals (12, 24, and 48 h), during the course of reduction. A bright green emission from AuNCs at 510 nm. (b) Lifetime measurements for AuNCs. (c) AuNC was excited with an UV hand light (365 nm) at different incubation time and shows a gradual red shift.

mounting medium to prevent fading and drying, followed by their observation with confocal laser scanning microscopy (CLSM). It was observed that most of the particles were uptaken by cells as the images were much brighter when compared to the control one.

3. RESULTS AND DISCUSSION

The Au(I)−thiolate intermediate was characterized by positive-ion electrospray ionization mass spectrum (ESI-MS) analysis. A peak at m/z = 1621.13 confirmed the formation of a tetranuclear gold cluster $[C_{32}H_{40}Au_4N_{20}S_4]$ (Supporting Information, Figure S3). The FTIR spectrum of 8-mercapto-9-propyladenine shows a band at 2674 cm^{-1} corresponds to S−H stretching in mercaptopurine,[38] whereas after AuNC formation this stretching band disappeared perhaps due to binding of thiol to the gold surface (Figure 1a). ^1H NMR also confirmed the disappearance of the S−H proton after AuNC formation (Supporting Information, Figure S4). PXRD of AuNCs shows the crystalline nature of the cluster and matched with the face-centered cubic structure of metallic gold (Figure 1b). MALDI-TOF mass spectra showed a peak of very weak intensity at m/z = 2711.597, corresponding to the $[Au_{13}S_4Na]^+$ cluster (calculated value = 2711.443).

The weak intensity of the $[Au_{13}S_4Na]^+$ cluster is perhaps due to extensive fragmentation at high laser intensity, resulting in peaks of lower molecular weight duly assigned as $[Au_{12}S_3]$, $[Au_{11}Na]^+$, $[Au_8S_9Na]^+$, $[Au_7S_4Na]^+$, $[Au_6S_7]^+$, $[Au_6S_3]^+$, and $[Au_5S_5Na]^+$ clusters (Figure 1c). TEM micrograph shows ultrafine monodispersed AuNCs of size ∼2 nm (Figure 1d). Dynamic light-scattering measurements on AuNCs further confirmed the formation of smaller size clusters with an average hydrodynamic diameter of 2.6 ± 0.7 nm (Figure 1e). UV−vis absorption spectrum shows an absorption band around 280−

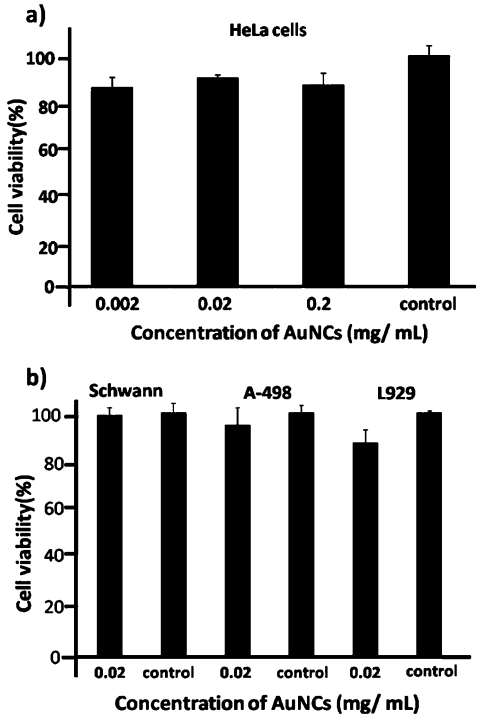

Figure 3. MTT cytotoxicity assay of AuNCs (a) with HeLa cells and (b) with Schwann, A498, and L929 cell lines.

dx.doi.org/10.1021/am405345h | ACS Appl. Mater. Interfaces 2014, 6, 2185−2191

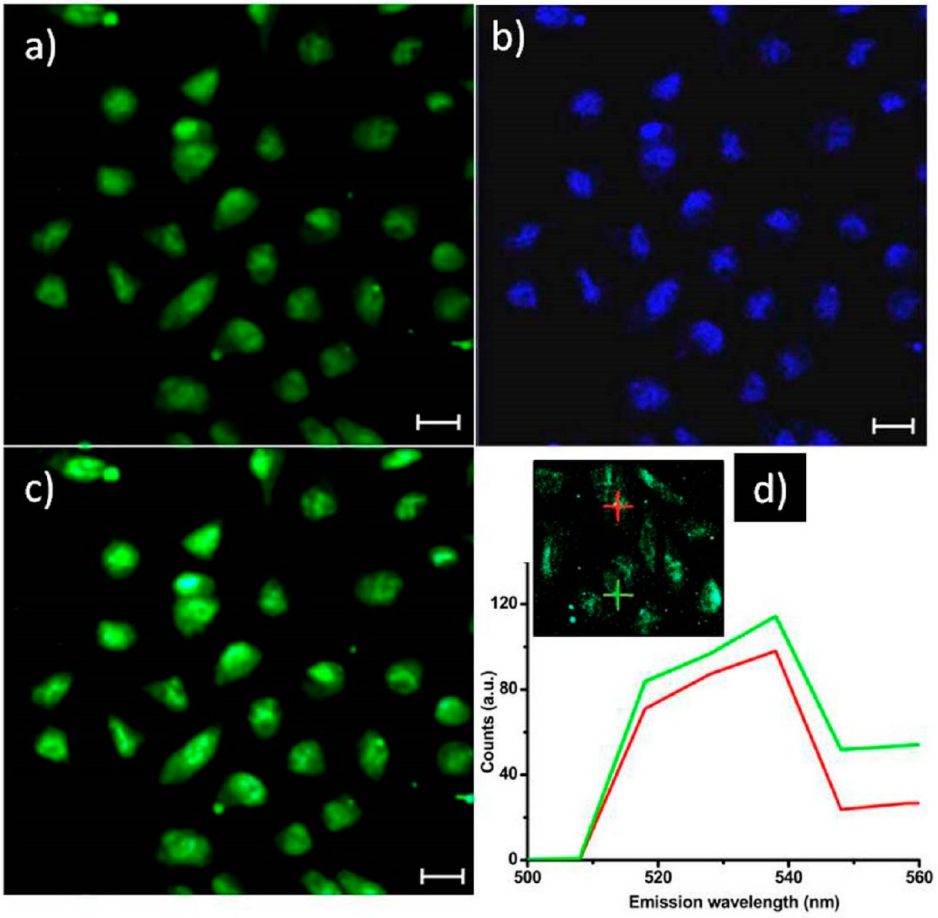

Figure 4. Confocal laser scanning microscope images of HeLa cells (a) after treatment with AuNCs; (b) after staining with Hoescht 33258 dye. (c) Merged image of (a) and (b). (d) Luminescence spectra taken on the cell surface at two different points (red, green markers) matched with the observed fluorescence of AuNCs (scale bar corresponds to 10 μm).

330 nm (Supporting Information, Figure S5). The absence of a plasmon resonance band at 520−530 nm confirms the formation of AuNCs instead of gold nanoparticles.[39]

Fluorescence emission spectra of the reaction mixture taken over different time intervals, during the course of reduction, exhibit a distinct red shift from blue-to-green emission (Figure 2a,c). The fluorescence emission spectra recorded at different time intervals reveal complete reduction of the Au(I)−thiolate complex to AuNCs, over a period of 48 h. When AuNCs were excited at 330 nm, a broad emission band was observed with $\lambda_{max} \approx 510$ nm. This observed emission matches with photophysical properties of Au_{13} clusters reported in the literature.[40] Lifetime measurements showed that the cluster possesses a lifetime of ∼0.5 ns (Figure 4b). Quantum yield (QY) of AuNCs was determined by using quinine sulfate in 0.5 M sulfuric acid as a reference.[41] QY of AuNCs was found to be ∼1.2% in methanol.

The chemical stability of AuNCs was also determined at different salt concentrations (154 mM NaCl, 0.5 M NaCl, 1 M NaCl, and PBS buffer, pH 7.4). After 24 h incubation, the UV−visible absorbance and emission spectrum of AuNCs did not show any significant change suggesting high chemical stability of AuNCs at varied salt concentrations (Supporting Information, Figure S6). We further investigated the photostability of AuNCs over a period of 6 months and observed persistent bright green emission (Supporting Information, Figure S7).

Superior photostability and chemical stability of these AuNCs prompted us to investigate their bioimaging application. Cancerous cell lines such as HeLa (malignant immortal cell line derived from cervical cancer), A498 (human kidney carcinoma cell line), noncancerous neuronal Schwann cells (causes nerve sheath tumor and nonmalignant), and L929 cells (derived from mouse fibroblast cells) were chosen for the biocompatibility and uptake studies. MTT assay was performed for HeLa cells with three different concentrations (0.002−0.2 mg/mL) of AuNCs. The results clearly suggested that these nanoclusters are highly biocompatible not only with HeLa cells (Figure 3a) but also with the other three cell lines at 0.02 mg/mL concentration (Schwann, A498, and L929) (Figure 3b).

HeLa cells (10^4 cells/well) were treated with 0.02 mg/mL of AuNCs for 16 h to investigate their cellular uptake and fluorescence imaging capability. The confocal laser scanning microscopy image of HeLa cells with AuNCs and localized bright green fluorescence from the cells clearly suggests that the nanoclusters were efficiently internalized by these cells (Figure 4). From CLSM images, it is also evident that the bright green emission arises from the nucleus. This was further confirmed by staining of the nucleus with Hoechst dye in which the localized bright green emission (Figure 4a) and blue emission (Figure 4b) arise from the same location. The merged image (Figure 4c) also proves the above observation. This clearly supports that the green fluorescent AuNCs stain the nucleus with high specificity, which may be due to the presence of 8-mercapto-9-

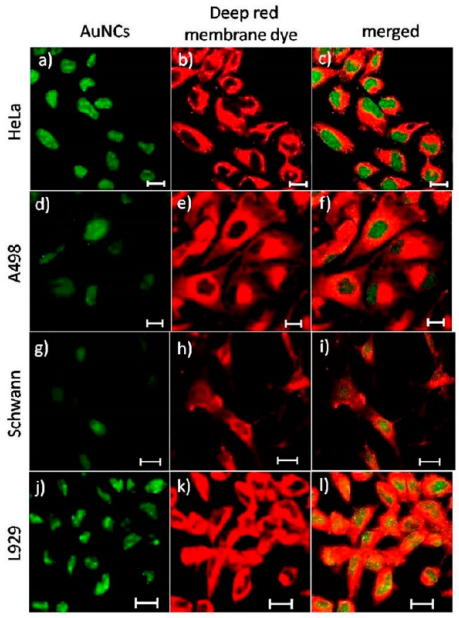

Figure 5. Confocal laser scanning microscope images of four different cell lines after treatment with green emitting AuNCs (λ_{em} = 510 nm); deep red plasma membrane dye exhibits red emission (λ_{em} = 633 nm), which is used as a reference for cell membrane staining. (a–c) Images of AuNCs, deep red plasma membrane dye, and their merged images of HeLa cells, respectively. (d–f) Images of A498 cells; (g–i) images of Schwann cells; (j–l) images of L929 cells (scale bar corresponds to 10 μm).

propyladenine purine base over the surface of nanoclusters. The corresponding fluorescence spectrum collected from the nucleus matches with the fluorescence spectrum of as-prepared AuNCs (Figure 4d). We note that the very weak green emission that arises from the other intracellular compartments is due to the background signal (Supporting Information, Figure S8).

In a control experiment, HeLa cells were incubated with 8-mercapto-9-propyladenine alone, where no green emission was observed (Supporting Information, Figure S9). In another experiment, treatment of HeLa cells with 8-mercapto-9-propyladenine for 4 h, followed by the addition of AuNCs, resulted in a very weak green emission from the cell nuclei suggesting an intriguing role of 8-mercapto-9-propyladenine in nuclei staining (Supporting Information, Figure S9).

To confirm generality of nuclei targeting ability, AuNCs were incubated with three different cell lines: A498, Schwann, and L929 cells. The deep red plasma membrane dye was added to differentiate the cell membrane from other cell compartments, and confocal laser scanning microscopy images of cell lines incubated with AuNCs clearly showed green emission from their nuclei (Figure 5). These observations confirm that these AuNCs could specifically stain the nucleus of various cell types.

To dissect a possible uptake mechanism, different inhibitors that inhibit specific endocytic pathways were used in this study. We have used filipin III and genistein (inhibits caveolar-mediated pathway), chloropromazine and nocodazole (inhibits clatherin-mediated pathway), rottlerin (inhibits macropinocytosis), and cytochalasin-D (inhibits actin polymerization) inhibitors. HeLa cells (10^4 cells/well) were pretreated with inhibitors for 1 h, and then AuNCs were incubated with cells for 4 h. As a positive control, HeLa cells without inhibitor treatment were also employed for AuNC uptake. CLSM images

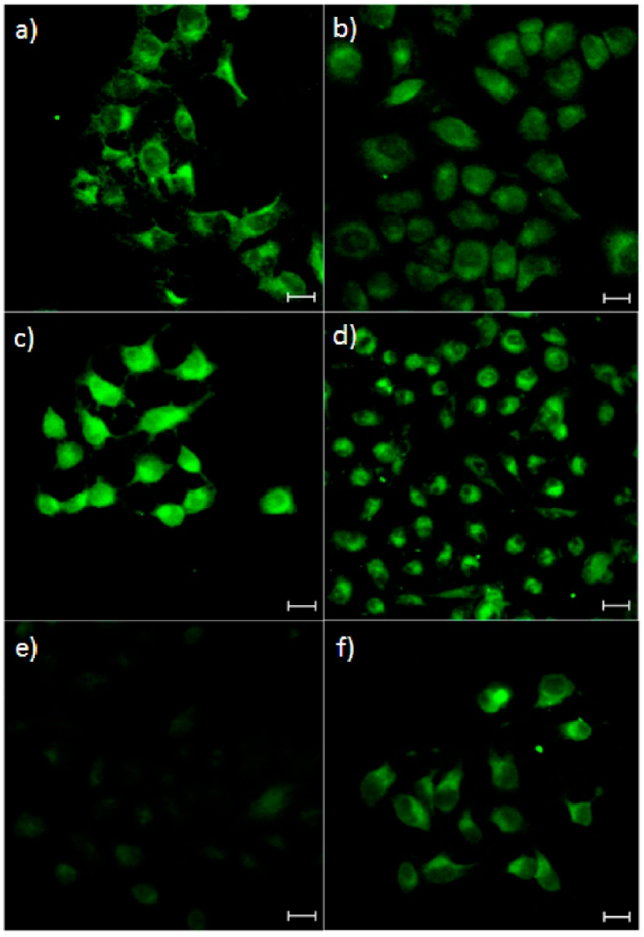

Figure 6. Confocal laser scanning microscopy images show a cellular uptake mechanism of AuNCs in HeLa cells. (a–f) Uptake inhibitions were screened with chlorpromazine, nocodazole, cytochalasin D, filipin, rottlerin, and genistein, respectively. Rottlerin (e) shows the most significant inhibition, suggesting AuNC internalization through the macropinocytosis pathway (scale bar corresponds to 10 μm).

(Figure 6) indicate much less uptake of AuNCs by cells treated with rottlerin, suggesting possible involvement of the macropinocytosis pathway in the uptake of newly synthesized AuNCs.[42,43]

4. CONCLUSIONS

In conclusion, we have demonstrated a simple method for preparing water-soluble bright green fluorescent 8-mercapto-9-propyladenine-capped gold nanoclusters (AuNCs), and it showed high chemical and photostability. Purine-capped nanoclusters exhibit high specificity to stain nuclei of various cell lines. We have also probed the pathway of AuNC internalization, where studies indicate the involvement of the macropinocytosis pathway for cell uptake of gold nanoclusters. Further applications of these photostable AuNCs are being envisaged.

■ ASSOCIATED CONTENT

Supporting Information

^{1}H NMR, ESI-MS, UV–vis spectra, chemical stability, and quantum yield calculation for gold nanoclusters. This material is available free of charge via the Internet at http://pubs.acs.org.

AUTHOR INFORMATION

Corresponding Authors

*E-mail: srisiva@iitk.ac.in. Tel.: +91 512 259 7697.
*E-mail: sverma@iitk.ac.in. Tel.: +91 512 259 7643.

Notes

The authors declare no competing financial interest.

ACKNOWLEDGMENTS

The authors would like to thank Prof. A. Sharma and S. Ganesh, IIT Kanpur, for providing cell lines used in this study. V.V. is thankful to UGC for fellowship, and S.S. is thankful to DBT for funding. S.V. is thankful to DAE for DAE-SRC Outstanding Investigator Award and DST for J C Bose National Fellowship.

DEDICATION

This paper is dedicated to Dr. Ganesh Pandey on the occasion of his 60th birthday.

REFERENCES

(1) Dam, D. H. M.; Lee, J. H.; Sisco, P. N.; Co, D. T.; Zhang, M.; Wasielewski, M. R.; Odom, T. W. *ACS Nano* **2012**, *4*, 3318−3326.
(2) Shang, L.; Dong, S.; Nienhaus, G. U. *Nano Today* **2011**, *6*, 401−418.
(3) Shang, L.; Dorlich, R. M.; Brandholt, S.; Schneider, R.; Trouillet, V.; Bruns, M.; Gerthsen, D.; Nienhaus, G. U. *Nanoscale* **2011**, *3*, 2009−2014.
(4) Bian, P.; Zhou, J.; Liu, Y.; Ma, Z. *Nanoscale* **2013**, *5*, 6161−6166.
(5) Chan, W. C.; Maxwell, D. J.; Gao, X.; Bailey, R. E.; Han, M.; Nie, S. *Curr. Opin. Biotechnol.* **2002**, *13*, 40−46.
(6) Luo, S.; Zhang, E.; Su, Y.; Cheng, T.; Shi, C. *Biomaterials* **2011**, *32*, 7127−7138.
(7) Wu, P.; Yan, X. P. *Chem. Soc. Rev.* **2013**, *42*, 5489−5521.
(8) Hardman, R. *Environ. Health Perspect.* **2006**, *114*, 165−172.
(9) Roberts, J. R.; Antonini, J. M.; Porter, D. W.; Chapman, R. S.; Scabilloni, J. F.; Young, S. H. *Part. Fibre Toxicol.* **2013**, *10*, 1−17.
(10) Resch-Genger, U.; Grabolle, M.; Cavaliere-Jaricot, S.; Nitschke, R.; Nann, T. *Nat. Methods* **2008**, *5*, 763−775.
(11) Ritchie, C. M.; Johnsen, K. R.; Kiser, J. R.; Antoku, Y.; Dickson, R. M.; Petty, J. T. *J. Phys. Chem. C* **2007**, *111*, 175−181.
(12) Wang, H. H.; Lin, C. A. J.; Lee, C. H.; Lin, Y. C.; Tseng, Y. M.; Hsieh, C. L.; Chen, C. H.; Tsai, C. H.; Hsieh, C. T.; Shen, J. L.; Chan, W. H.; Chang, W. H.; Yeh, H. I. *ACS Nano* **2011**, *5*, 4337−4344.
(13) Zhu, Y.; Qian, H.; Drake, B. A.; Jin, R. *Angew. Chem., Int. Ed.* **2010**, *49*, 1295−1298.
(14) Li, G.; Qian, H.; Jin, R. *Nanoscale* **2012**, *4*, 6714−6717.
(15) Kumara, S.; Jin, R. *Nanoscale* **2012**, *4*, 4222−4227.
(16) Chen, W. Y.; Lan, G. Y.; Chang, H. T. *Anal. Chem.* **2011**, *83*, 9450−9455.
(17) Tu, X.; Chen, W.; Guo, X. *Nanotechnology* **2011**, *22*, 095701−095707.
(18) Shang, L.; Yang, L.; Stockmar, F.; Popescu, R.; Trouillet, V.; Bruns, M.; Gerthsen, D.; Nienhaus, G. U. *Nanoscale* **2012**, *4*, 4155−4160.
(19) Shichibu, Y.; Konishi, K. *Small* **2010**, *6*, 1216−1220.
(20) Wan, X. K.; Lin, Z. W.; Wang, Q. M. *J. Am. Chem. Soc.* **2012**, *134*, 14750−14752.
(21) Zhu, M.; Aikens, C. M.; Hollander, F. J.; Schatz, G. C.; Jin, R. *J. Am. Chem. Soc.* **2008**, *130*, 5883−5885.
(22) Qian, H.; Eckenhoff, W. T.; Zhu, Y.; Pintauer, T.; Jin, R. *J. Am. Chem. Soc.* **2010**, *132*, 8280−8281.
(23) Jadzinsky, P. D.; Calero, G.; Ackerson, C. J.; Bushnell, D. A.; Kornberg, R. D. *Science* **2007**, *318*, 430−433.
(24) Chevrier, D. M.; Chatt, A.; Zhang, P. *J. Nanophotonics* **2012**, *6*, 064504−1−064504−16.
(25) Chen, Y.; Wang, Y.; Wang, C.; Li, W.; Zhou, H.; Jiao, H.; Lin, Q.; Yu, C. *J. Colloid Interface Sci.* **2013**, *396*, 63−68.
(26) Liu, C. L.; Wu, H. T.; Hsiao, Y. H.; Lai, C. W.; Shih, C. W.; Peng, Y. K.; Tang, K. C.; Chang, H. W.; Chien, Y. C.; Hsiao, J. K.; Cheng, J. T.; Chou, P. T. *Angew. Chem., Int. Ed.* **2011**, *50*, 7056−7060.
(27) Liu, G.; Shao, Y.; Ma, K.; Cui, Q.; Wu, F.; Xue, S. *Gold Bull.* **2012**, *45*, 69−74.
(28) Chen, H.; Li, B.; Wang, C.; Zhang, X.; Cheng, Z.; Dai, X.; Zhu, R.; Gu, Y. *Nanotechnology* **2013**, *24*, 055704.
(29) Kawasaki, H.; Hamaguchi, K.; Osaka, I.; Arakawa, R. *Adv. Funct. Mater.* **2011**, *21*, 3508−3515.
(30) Negishi, Y.; Takasugi, Y.; Sato, S.; Yao, H.; Kimura, K.; Tsukuda, T. *J. Am. Chem. Soc.* **2004**, *126*, 6518−6519.
(31) Zhang, H.; Liu, Q.; Wang, T.; Yun, Z.; Li, G.; Liu, J.; Jiang, G. *Anal. Chim. Acta* **2013**, *770*, 140−146.
(32) Kennedy, T. A. C.; MacLean, J. L.; Liu, J. *Chem. Commun.* **2012**, *48*, 6845−6847.
(33) Barman, A. K.; Chaturbedi, A.; Subramaniam, K.; Verma, S. *J. Nanopart. Res.* **2013**, *15*, 2083−2086.
(34) Venkatesh, V.; Kumar, J.; Verma, S. *CrystEngComm.* **2011**, *13*, 6030−6032.
(35) Hirota, K.; Kazaoka, K.; Sajiki, H. *Bioorg. Med. Chem.* **2003**, *11*, 2715−2722.
(36) Negishi, Y.; Nobusada, K.; Tsukuda, T. *J. Am. Chem. Soc.* **2005**, *127*, 5261−5270.
(37) Tim, M. *J. Immunol. Methods* **1983**, *65*, 55−63.
(38) Viudez, A. J.; Madueno, R.; Pineda, T.; Blazquez, M. *J. Phys. Chem. B* **2006**, *110*, 17840−17847.
(39) Qiao, J.; Mu, X.; Qi, L.; Deng, J.; Mao, L. *Chem. Commun.* **2013**, *49*, 8030−8032.
(40) Zheng, J.; Zhang, C.; Dickson, R. M. *Phys. Rev. Lett.* **2004**, *93*, 077402−1−077402−4.
(41) Brouwer, A. M. *Pure Appl. Chem.* **2011**, *83*, 2213−2228.
(42) Yang, L.; Shang, L.; Nienhaus, G. U. *Nanoscale* **2013**, *5*, 1537−1543.
(43) Levy, R.; Shaheen, U.; Cesbron, Y.; See, V. *Nano Rev.* **2010**, *1*, 4889−4907.